Available online at www.sciencedirect.com

ScienceDirect

journal homepage: www.elsevier.com/locate/he

Absorption and desorption of hydrogen in long metal hydride tank equipped with phase change material jacket

A. Ali Rabienataj Darzi [a,*], H. Hassanzadeh Afrouzi [b], A. Moshfegh [c], M. Farhadi [b]

[a] Department of Mechanical Engineering, University of Mazandaran, P.O. Box: 416, Babolsar, Iran
[b] Faculty of Mechanical Engineering, Babol University of Technology, Babol, Iran
[c] School of Aerospace, Mechanical, and Mechatronic Eng., University of Sydney, NSW 2006, Australia

ARTICLE INFO

Article history:
Received 14 January 2016
Received in revised form
7 April 2016
Accepted 8 April 2016
Available online 28 April 2016

Keywords:
Metal hydride tank
Hydrogen storage
Phase change material

ABSTRACT

A numerical study was carried out to address the practical aspects of hydrogen absorption and desorption process in a long tubular $LaNi_5$ metal hydride tank (MHT) integrated with Rubitherm phase change material (PCM) jacket for hydrogen supplying of PEM fuel cell. Different H_2 supply pressures ($p = 10$, 15 and 20 bar), different discharge pressures ($p = 1.5$, 1.75 and 2 bar) and metal hydride bed porosities (0.4, 0.5 and 0.6) were rigorously analyzed to report their influences on transient and local temperature distributions across H_2-MHT system and PCM jacket. The time-dependent changes of hydrogen to metal (H/M) ratio and PCM melt fraction were also investigated until they reach equilibrium. It was found that system temperature, PCM melt fraction and H/M ratio reach steady state with different rates, such that systems with higher supply pressure in absorption, lower discharge pressure in desorption and higher bed porosity approach steady state faster. Up to the steady state, 64%, 79% and 91% of the initial volume of solid PCM liquefies in absorption and 67%, 83% and 95% of liquid PCM solidifies in desorption for bed porosities of 0.6, 0.5 and 0.4, respectively. The MHT is charged with hydrogen much faster under high supply pressures. Also, it is discharged much faster under lower discharge pressure. Inserting metal foam in the PCM jacket enhances the thermal conductivity, and significantly reduces the charging and discharging time.

Start of the Assignment
(1/3) Reduce to one (single) spatial dimension;
(2/3) Discretize is space using finite difference method on a uniform mesh;
(3/3) Solve in time using a ODE solver;

Introduction

Growing environmental crises such as ozone layer depletion, emission of greenhouse gasses (carbon dioxide, methane, nitrous oxide, and fluorinated gases), and the air pollution by fossil fuels, have attracted vast attentions to substitute the gasoline by renewable and green energy solutions such as hydrogen (H_2). Hydrogen-driven fuel cells, namely alkaline fuel cell and proton exchange membrane fuel cell, are not yet commercially viable due to existing problems in storing the hydrogen. The solid-state metal hydride material has advantages in comparison with the conventional compressed

* Corresponding author. Tel.: +98 113 5302902.
E-mail addresses: a.rabienataj@umz.ac.ir, ar.darzi@yahoo.com (A.A. Rabienataj Darzi), hamidhasanzade@yahoo.com (H. Hassanzadeh Afrouzi), abouzar.moshfegh@sydney.edu.au (A. Moshfegh), mfarhadi@nit.ac.ir (M. Farhadi).
http://dx.doi.org/10.1016/j.ijhydene.2016.04.051

Nomenclature

C	heat capacity, J/kg K
C'	mushy zone constant, kg/m^{3}s
C_a	absorption rate coefficient, s^{-1}
C_d	desorption rate coefficient, s^{-1}
C_p	heat capacity at constant pressure, J/kg K
E_a	activation energy for absorption, J/mole
E_d	activation energy for desorption, J/mole
H/M	hydrogen to metal atomic ratio
K	permeability, m^2
K	thermal conductivity, W/m K
l	length of reactor, m
$\dot{m}$	hydrogen mass reaction rate, Kg/m^{3}s
P	absolute pressure, Pa
R_1	radius of inlet, m
R_2	radius of metal hydride tank, m
R_3	radius of PCM Jacket, m
R	universal gas constant, J/mole K
t	time, s
T	temperature, K
U	velocity, m/s
S	source term
H	total enthalpy, J/kg
h	sensible enthalpy, J/kg

Greek letters

ρ	density, kg/m^3
μ	dynamic viscosity, kg m^{-1}s
β	melt fraction
ΔH	enthalpy of absorption, J/mole
ΔH_p	latent heat content, J/kg

Subscripts

0	initial
a	absorption
d	desorption
eq	equilibrium
eff	effective
g	gas
in	inlet
l	liquid PCM
p	PCM in both phases
P	constant pressure
r	r-coordinate
ref	reference
s	solid bed
sat	saturate
sp	solid PCM
z	z-coordinate

gaseous or liquid H_2 cylinders in vehicular applications. High gravimetric and volumetric density, high H_2 absorption capacity, moderate working temperature and moderate charging pressure for H_2 storage, all make the metal hydride tanks (MHT) a considerable choice. Compact size and energy efficiency of metal hydride fuel cells are capable to make them superior choices to batteries in portable applications.

During the last two decades, there have been studies on key parameters such as metal hydride bed kinetic reaction, heat and mass transfer rates of hydrogen that all play significant roles in performance of hydrogen charging process. Several numerical and experimental studies have been performed to develop two-dimensional models of MHTs, and determine the reaction kinetics and equilibrium pressure for $LaNi_5$ hydrogen storage system [1–3]. Muthukumar et al. [4] carried out a numerical investigation on hydrogen absorption performance of $MmNi_{4.6}Al_{0.4}$ storage tanks. They studied the effects of different supply pressures, overall heat transfer coefficients and wall temperatures on the reaction rate between H_2 and metal alloy. Results indicated that increasing the overall heat coefficient up to 1250 w/m^{2}K does not accelerate the absorption time because of high thermal resistance of metal hydride bed. Muthukumar and Ramana [5] studied the effects of different wall boundary conditions and bed thicknesses on H_2 desorption process. They indicated that discharging time mainly depends on the successful heat removal from the bed.

Absorption of hydrogen into metal alloys expands and rearranges its crystalline structure and forms the metal hydride medium. The formation of new bonds generates extra heat that must be removed to an external source. In turn the hydrogen desorption or discharge process requires breaking of bonds, compression of the crystal and hence the heat is sunk from environment. Therefore heat transfer during charge/discharge processes, as the challenging obstacle in utilizing the metal hydride tanks as hydrogen storage, has focused the attentions on integration of MHTs with various heat exchangers. A spiral heat exchanger was designed for a metal hydride tank by Mellouli et al. [6]. Their experimental results showed that the charge/discharge times of the reactor are considerably reduced when a heat exchanger is used. Dhaou et al. [7] utilized a finned spiral heat exchanger to improve the heat transfer and reduce the hydrogen charging time significantly compared to typical spiral heat exchangers. Muthukumar et al. [8] numerically studied the absorption process inside the $MmNi_{4.6}Al_{0.4}$ metal hydride tank equipped with internal cooling tubes and external cooling jacket. Based on the developed 2D mathematical model in cylindrical coordinates, they considered different numbers and various arrangements of cooling tubes to obtain the optimum geometry associated with the minimum absorption time. Askri et al. [9] employed a numerical model to study the hydrogen charge process behavior in different geometries of metal hydride and heat exchangers. They showed that a concentric heat exchanger tube equipped with fins yields efficient absorption rate for hydrogen. McDonald and Rowe [10] also studied the improvements on the external heat transfer from MHTs by attaching additional fins.

Many numerical simulations are implemented to model and economize the heat transfer from metal hydride storages, and hence to reduce the hydrogen absorption time. Freni et al. [11] carried out a computational study on cooling of $LaNi_5$

hydrogen storage systems by means of finite element method. They considered two different cooling systems consisting of internal cooling tubes and an external cooling jacket with cooling inner tubes to enhance the heat transfer from the metal bed. They found that the dual heat transfer system with outer jacket and inner tubes improves the performance of metal hydride charging process. Their results also showed that the thermal conductivity and permeability of the metal hydride bed are important factors for an optimized design of MHTs. Chung et al. [12] performed an experimental study on the absorption rates of hydrogen into the MHT equipped with heat pipes for heat transfer augmentation. The results revealed that absorption time was reduced by half.

Even though the integration of heat exchangers represents an active heat transfer method to accelerate charge/discharge processes inside the metal hydride tanks, it requires some considerations such as designing a complex system for heat removal/supply in heat exchangers. Thus, an effective passive heat transfer system could be a viable solution for cooling of metal hydride tanks during the charge process without the need for external energy. Phase change materials (PCMs) absorb a large amount of energy as latent heat at a constant phase transition temperature, and are capable to release it afterward. These materials, e.g. paraffins, salt hydrates a metallic PCMs can be used for passive heat storage or cooling source [13–15]. Distinctive properties of PCMs include heat sink at constant temperature, heat recovery with small temperature drop, high heat storage capacity, melting point which matches the applications and chemical stability which allows the PCM to be utilized in many industrial applications such as thermal storage of solar energy [16], cooling of electronic devices [17,18] and thermal management of building [19]. The melting and solidification of PCMs have been studied in the literature mainly to predict the time required for heat storage and release [20–24]. Recently, phase change materials have been used for cooling or heating of metal hydride tank. Garrier et al. [25] carried out an experimental study on desorption of hydrogen from MgH_2 tank integrated with PCM. They reported that desorption process takes 3 h for releasing the 7050 NL hydrogen, and the daily storage efficiency was recorded as 70%. Mellouli et al. [26] performed a numerical study on absorption and desorption process inside MgH_2 small tank equipped with high temperature PCM. Their result showed that the use of a PCM could be a potential candidate for the metal hydride storage units. Ben Mâad et al. [27] carried out a numerical study by finite element method on absorption of hydrogen in metal hydride tank equipped with PCM jacket. They investigated the effects of thermal conductivity and latent heat of PCM on hydrogen reaction rate and PCM melting rate. Ben Mâad et al. [28] extended their previous numerical study on absorption and desorption of hydrogen in $LaNi_5$ metal hydride tank integrated with PCM. Their result indicated that the metal hydrogen reactor can evacuate up to 80% of the hydrogen stored by implementation of PCM without auxiliary heat source.

Based on the surveyed literature, there still exist unrevealed physical correlations and shortcomings in numerical modeling that we attempt to address them thoroughly. They are: 1- the analytic relation (Heaviside step function) were used to find the liquid fraction of PCM where it calculated computationally in present study, 2- PCM used in the previous works have high volume expansion during phase change while it was not considered in simulations. Here a PCM with almost negligible expansion during phase change is selected, 3- we consider the resistance of hydrogen flow in a long metal bed by solving momentum equation in full mode while it was neglected in previous works for small tanks.

Present study investigates the cooling and heating of a cylindrical $LaNi_5$ metal hydride tank using an annular jacket filled by commercially available Rubitherm phase change material. The simulation of hydrogen charge and discharge processes into the $LaNi_5$ porous bed is coupled with the heat transfer to the PCM jacket. The system time-dependent thermal response is compared against experiment to verify the fidelity of numerical schemes adopted. The temporal temperature variations of metal hydride bed and hydrogen together with the PCM are analyzed across a range of supply pressures and bed porosities. The changes of PCM liquid fraction as the indicative role player in heat absorption and desorption capacity are also monitored as the system approaches the steady state. To quantify the H_2 absorption rate, hydrogen to metal (H/M) bed volumetric ratio is plotted versus time at various inlet pressures. It is also studied that how the porosity of metal hydride bed and enhancing the thermal conductivity of PCM by inserting metal foam affect the system temperature, PCM melt fraction and H/M ratio.

Governing equations

Metal hydride porous bed

Fig. 1 shows the schematic of concentric tubes geometry for the metal hydride tank and the surrounding cooling jacket packed with PCM. The alloy bed material is considered to have the $LaNi_5$ properties (see Table 1). $LaNi_5$ has wide practical applications because of its high absorption capacity, easy activation, moderate hysteresis, stable performance, and rapid absorption and desorption rates [29–32]. The

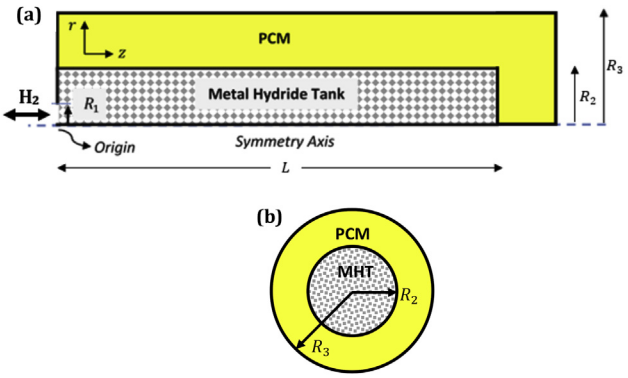

Fig. 1 – Schematics of simulation geometry for the cylindrical metal hydride tank encircled by a jacket packed with phase change material as the heat absorbent: (a) longitudinal view; (b) cross-sectional view. The hydrogen inlet and other dimensions are shown.

Table 1 – Thermal and physical properties of $LaNi_5$ metal hydride bed and hydrogen [1].

Parameter	Description	Value
C_a	Absorption rate coefficient	59.187 s^{-1}
C_d	Desorption rate coefficient	9.57 s^{-1}
C_{pg}	Heat capacity of hydrogen	14,890 J/mol K
C_{ps}	Heat capacity of metal	419 J/kg K
E_a	Activation energy in absorption	21179.6 J/mol
E_d	Activation energy in desorption	16,473 J/mol
K	Permeability	10^{-9} m^2
k_g	Hydrogen thermal conductivity	0.1815 W/(m K)
k_{MH}	Metal bed thermal conductivity	2 W/(m K)
M_g	Hydrogen molecular weight	2.016 kg/kmol
ε	Porosity	0.4, 0.5, 0.6
ρ_{emp}	Empty bed density	7164 kg/m3
ρ_{sat}	Saturated bed density	7259 kg/m^3
ν_g	Hydrogen viscosity	8.4×10^{-6} kg/(m s)

hydrogen is injected or extracted from the small opening with the radius $R_1 = 1$ cm located on the axis of inner tube. The length and radius of cylindrical metal hydride tank are taken 80 cm and 4 cm respectively. The annular cooling/heating jacket has the outer radius $R_3 = 7$ cm that yields a net thickness of 3 cm for the PCM jacket enclosure. The required amount of PCM for determining the jacket volume was calculated by estimating the heat generated in or released from MH tank (see Eq. (19)).

The main assumptions considered in developing the model are:

a) The gas phase behaves as a thermodynamically ideal gas.
b) The solid phase is isotropic and has a uniform porosity.
c) The media is in local thermal equilibrium.
d) Thermal–physical properties are constant.
e) The MHT-PCM system is adiabatic (zero heat loss/gain from ambient).
f) Equilibrium gas pressure is calculated by Van't Hoff equation [33].

The governing equations for hydrogen mass, momentum and heat transfer coupled with the kinetic reaction of absorption in the metal hydride bed are introduced below. Changes of solid density for the reacting porous metal bed, and the mass flow rate for hydrogen are respectively given by:

$$(1-\varepsilon)\frac{\partial \rho_s}{\partial t} = \dot{m} \tag{1}$$

$$\varepsilon\frac{\partial \rho_g}{\partial t} + \frac{1}{r}\frac{\partial}{\partial r}\left(r\rho_g u_r\right) + \frac{\partial}{\partial z}\left(\rho_g u_z\right) = \dot{m} \tag{2}$$

where ρ stands for density and the subscripts s and g represent the solid (bed) and gas (hydrogen), ε is the metal bed porosity, m denotes the mass of absorbed hydrogen in both equations, t is time for the transient absorption process, r and z are radial and longitudinal coordinates, and u is the velocity of hydrogen flow. The hydrogen absorption and desorption mass rate are given by:

Do both \rho_s and \rho_g increase or decrease at the same time?

$$\dot{m} = C_a \exp\left(-\frac{E_a}{RT}\right)\ln\left(\frac{p_g}{p_{eq,a}}\right)(\rho_{sat} - \rho_s) \tag{3}$$

$$\dot{m} = C_d \exp\left(-\frac{E_d}{RT}\right)\left(\frac{p_g - p_{eq,d}}{p_{eq,d}}\right)\left(\rho_s - \rho_{emp}\right) \tag{4}$$

where C_a and C_d are the absorption rate and desorption rate coefficients, E_a and E_d are the absorption and desorption activation energies, respectively, R is the universal gas constant, ρ_{sat} is the saturation density of metal, ρ_{emp} is the Hydrogen-free metal hydride density and p_{eq} stands for bed equilibrium pressure. Van't Hoff equation relates the equilibrium pressure (p_{eq}) and reference pressures (p_{ref}) to hydrogen-MHT equilibrium temperature (T) as given below [33].

$$Ln\left(\frac{P_{eq}}{P_{ref}}\right) = A - \frac{B}{T} \tag{5}$$

where p_{ref} is 1 MPa [33], and the constants A and B are set to 10.7 and 3704.6 for absorption and they are set to 10.57 and 3704.6 for desorption, respectively. These values are determined from the hydride material listing database [34]. Momentum equations for hydrogen flow along r and z directions are respectively explained by:

$$\rho_g\frac{\partial u_r}{\partial t} = -\frac{\partial p_g}{\partial r} - \rho_g\left(u_r\frac{\partial u_r}{\partial r} + u_z\frac{\partial u_r}{\partial z}\right) + \mu\left(\frac{\partial}{\partial r}\left(\frac{1}{r}\frac{\partial}{\partial r}(ru_r)\right) + \frac{\partial^2 u_r}{\partial z^2}\right) - S_r \tag{6}$$

$$\rho_g\frac{\partial u_z}{\partial t} = -\frac{\partial p_g}{\partial z} - \rho_g\left(u_r\frac{\partial u_z}{\partial r} + u_z\frac{\partial u_z}{\partial z}\right) + \mu\left(\frac{1}{r}\frac{\partial}{\partial r}\left(r\frac{\partial u_z}{\partial r}\right) + \frac{\partial^2 u_z}{\partial z^2}\right) - S_z \tag{7}$$

Here, S_r and S_z represent the pressure loss in the bed due to viscous dissipation. S_i in each direction is then calculated by:

$$S_i = \left(\frac{\mu}{K}\right)u_i \tag{8}$$

where K denotes the permeability of the porous bed and is obtained via:

$$K = \frac{\varepsilon^3 d^2}{150(1-\varepsilon)^2} \tag{9}$$

In above relation, d is the average diameter of opening in porous bed. Assuming the thermodynamic equilibrium between metal hydride bed and hydrogen, the system temperature can be expressed by one equation as

$$(\rho C_p)_{eff}\frac{\partial T}{\partial t} + \left(\varepsilon\rho_g C_{p,g} u_r \frac{\partial T}{\partial r}\right) + \left(\varepsilon\rho_g C_{p,g} u_z \frac{\partial T}{\partial z}\right) = \frac{1}{r}\frac{\partial}{\partial r}\left(r k_{eff}\frac{\partial T}{\partial r}\right) + \frac{\partial}{\partial z}\left(k_{eff}\frac{\partial T}{\partial z}\right) - \dot{m}\left((1-\varepsilon)\Delta H + T(C_{p,g} - C_s)\right) \tag{10}$$

where $C_{p,g}$ is the heat capacity of hydrogen in constant pressure, ΔH is the enthalpy difference of absorption, $(\rho C_p)_{eff}$ and k_{eff} are the effective volumetric heat capacity and effective thermal conductivity respectively which are averaged between bed and hydrogen via

$$(\rho C_p)_{eff} = \varepsilon\rho_g C_{p,g} + (1-\varepsilon)\rho_s C_s \tag{11}$$

$$k_{eff} = \varepsilon k_g + (1-\varepsilon)k_s \tag{12}$$

The thermal and physical properties of metal hydride bed and hydrogen used in above formulations are tabulated in Table 1.

The interface between PCM jacket and metal hydride tank is considered to be an aluminum wall with the thickness of 3 mm. To compute the thermal resistance of the wall, 1D conduction equation is solved in radial and vertical directions as follows

$$\left(\rho C_p\right)_{Al}\frac{\partial T}{\partial t} = \frac{k_{Al}}{r}\frac{\partial}{\partial r}\left(r\frac{\partial T}{\partial r}\right) \tag{13}$$

$$\left(\rho C_p\right)_{Al}\frac{\partial T}{\partial t} = k_{Al}\frac{\partial T}{\partial z} \tag{14}$$

PCM formulations

The PCM which is used for present configuration should have following characteristics.

1- Low volume expansion during phase change.
2- High latent heat of fusion to store or release high amount of thermal energy.
3- Adequate melting temperature (higher than ambient temperature and less than maximum/minimum temperature which is experienced by metal bed during absorption/desorption process).

The melting temperature should have a value higher than ambient temperature and less than maximum/minimum temperature which is experienced by metal bed during absorption/desorption process.

In this way, the commercially available Rubitherm (salt) SP29Eu was chosen as the phase change material. Thermophysical properties of SP29Eu are given in Table 2.

Natural convection term is ignored due to low thermal expansion of the PCM. The PCM solidification/melting process is modeled via the enthalpy-porosity technique [35,36] Rather than explicitly tracking the melt interface, this method assigns a liquid fraction to each computational cell based on the enthalpy balance. Thermal energy equations can be expressed as follows:

$$\frac{\partial}{\partial t}\left(\rho_p H_p\right) = k_p\left(\frac{1}{r}\frac{\partial}{\partial r}\left(r\frac{\partial T}{\partial r}\right) + \frac{\partial^2 T}{\partial z^2}\right) \tag{15}$$

In above conservation equations subscript p is proprietary to PCM and H_p is the total enthalpy which is defined as the sum of sensible enthalpy (h) and the latent heat content (ΔH_p) of PCM.

$$H_p = h + \Delta H_p, \tag{16}$$

The latent heat content of PCM (ΔH_p) may vary between zero (solid PCM) and L_p (liquid PCM). Therefore, PCM melt fraction β can be calculated via

$$\beta = \begin{cases} \dfrac{\Delta H_p}{L} = 0 & T < T_{sp} \\ \dfrac{\Delta H_p}{L} = 1 & T > T_l \\ \dfrac{\Delta H_p}{L} = \dfrac{T - T_{sp}}{T_l - T_{sp}} & T_{sp} < T < T_{sp} \end{cases} \tag{17}$$

where T_{sp} and T_l represent the solidus and liquidus temperatures of PCM. The latent heat content can now be written in terms of the latent heat of the PCM (L_p) and melt fraction (β) as:

$$\Delta H_p = \beta L_p \tag{18}$$

The volume of PCM jacket (V_P) is calculated as follows

$$V_P = \frac{\left(\rho_{ss} - \rho_{emp}\right)\varepsilon\,\Delta H\, V_{MH}}{\rho_P L_P} \tag{19}$$

where V_{MH} is the volume of metal bed. It should be noted that sensible enthalpy is ignored in the calculation of required PCM due to its small effect with respect to other terms.

Numerical schemes and validation

The set of coupled partial differential governing equations were solved by the commercial software Fluent™ v6.3.26 for which three User Defined Functions (UDFs) were developed to apply the source terms in mass and energy equations (Eq. (2) and Eq. (10)) as well as the equilibrium pressure (Eq. (5)). In order to solve the momentum and energy equations the

Table 2 – Thermo-physical properties of Rubitherm PCM (SP29Eu).

Melting temperature (K)	Density (kg/m^3)	Specific heat (J/kg K)	Thermal conductivity (W/m K)	Latent heat of fusion (J/kg)
302.15–304.15	2000	2500	0.6	175,000

power law differencing scheme [37], and for pressure–velocity coupling the PISO (Pressure implicit with splitting of operator) method [38] were used. Also the PRESTO (PREssure STaggering Option) scheme [37] was adopted for the pressure correction. The PCM solidification/melting process is modeled via the enthalpy-porosity technique. Rather than explicitly tracking the melt interface, this method assigns a liquid fraction to each computational cell based on the enthalpy balance.

To achieve a stable solution through iterations, the under-relaxation factors for both velocity components, pressure correction, thermal energy and liquid fraction were respectively set to 0.4, 0.3, 1 and0.9. Solution independency from mesh topology was examined by comparing the variations in hydrogen absorption rate and temperature over many grid sizes. An arrangement of 5250 structured grids was then found suitable to yield a grid-independent solution. At each time step sized at 0.01 s, a course of 40 iterations were found sufficient to satisfy the convergence criteria of 10^{-8} for energy equation and 10^{-5} for mass and momentum equations. The transient simulation was then ran up to 300 min for absorption process and 600 min for desorption process where system steady state is confidently reached.

The initial metal hydride density is taken as Hydrogen-free metal hydride density ($\rho_0 = \rho_{emp}$) for absorption case and it is taken as the saturate density ($\rho_0 = \rho_{sat}$) for desorption case. The initial temperature of system (PCM and Metal hydride tank) is taken as 301.15 and 305.15 K in absorption and desorption processes, respectively. Hydrogen pressure is assumed to be the equilibrium pressure at the initial temperature.

The boundary conditions are considered as follows:

$$P = P_{in/out} \quad at \quad z = 0, \quad 0 \le r \le R_1$$

$$\frac{\partial T}{\partial z} = 0, \; u_r = u_z = 0 \quad at \quad z = 0, \quad R_1 \le r \le R_2$$

$$\frac{\partial T}{\partial r} = 0, \; u_r = u_z = 0 \quad at \quad r = R_3, \; 0 \le z \le L$$

$$\frac{\partial T}{\partial z} = 0, \; u_r = u_z = 0 \quad at \quad z = L + R_2, \; 0 \le r \le R_3$$

$$\frac{\partial T}{\partial z} = 0, \; u_r = u_z = 0 \quad at \quad z = 0, \; R_2 \le r \le R_3$$

As mentioned earlier, the interface between PCM jacket and metal hydride tank is considered as an aluminum wall. One dimensional equations for conduction heat transfer is solved within the thin wall to compute the thermal resistance [53].

The set of suggested numerical schemes was verified against the experimental work of Jemni et al. [3] in a small reactor at hydrogen charge pressure of 10 bar and working temperatures of T = 293 K and 313 K for absorption. It was also verified against the study of Chung et al. [33] in the same reactor at discharge pressure of 0.1 MPa and working temperature of 313 K. Fig. 2 shows that the present model evaluates the bed temperature and H/M ratio with small deviation which confirms the fidelity of the simulation model for further investigations.

Further validation is performed against experimental work of Assis et al. [39] for melting of PCM inside spherical container for temperature difference of 10 K. A comparison of liquid fraction versus time between present simulation and Assis et al. [39] is shown in Fig. 3. It depicts that there is good agreement between those works.

Another verification is performed between present numerical simulation and Garrier et al. [25] experimental work on mgH_2 metal hydride tank equipped with PCM (Mg–Zn eutectic). Fig. 4 indicates that there is reasonable agreement between present simulation and experimental data [25].

Results and discussion

Simulations were conducted across the charging pressure range of 10–20 bar, the discharging pressure range of 1.5–2 bar and at three different metal bed porosities ($\varepsilon = 0.4$, 0.5 and 0.6) in long metal hydride tank equipped with phase change material jacket. In addition, the metal foam is inserted into jacket to enhance the thermal conductivity of PCM. We study the spatio-temporal variations in metal bed, hydrogen and PCM temperatures until they reach steady state and thermal equilibrium. Also the effects of metal bed porosity on the bed temperature, H/M ratio and PCM liquid fraction are thoroughly discussed.

Charging process

Fig. 5 shows the time-dependent variations of metal bed temperature for inlet pressures of 10, 15 and 20 bar and constant porosity of 0.5. At the beginning of absorption process, the temperature of metal bed increases abruptly due to the high reaction rate between hydrogen and MHT. High reaction rate induces high mass absorption rate for hydrogen and subsequently the source term $(\dot{m}(1-\varepsilon)\,\Delta H)$ in the energy equation (Eq. (10)) causes abrupt increase in the temperature. Due to the low thermal conductivity of metal hydride tank, heat transfer from MHT to PCM needs longer time than expected, hence the released energy as the result of fusion and re-arrangement of MHT molecular structure accumulates in system at early stages of the charge process. Similar trends for system temperature versus time have been also reported under high heat convection on the metal bed wall [40,41].

The prominent feature is the existence of an intersection point around $t = 110$ min where temperature change versus pressure follows different trends. For $t < 110$ min, the system temperature increases as the supply pressure gets higher, while for $t > 110$ min temperature becomes lower at higher pressures. High supply pressure induces a large pressure difference between the initially empty porous MHT and hydrogen flow so it intensifies the reaction rate. Therefore, cases with higher reaction rates (associated with larger slope in Fig. 5) can potentially absorb more hydrogen at the same time, and faster reach the steady state. Therefore, the heat released from the MHT at high supply pressures becomes lower than that at low supply pressures.

Fig. 6 depicts the temperature contours for MHT and PCM in both solid and liquid phases at supply pressure of 10 bar during the time interval $2 \le t \le 250$ min. At early times of

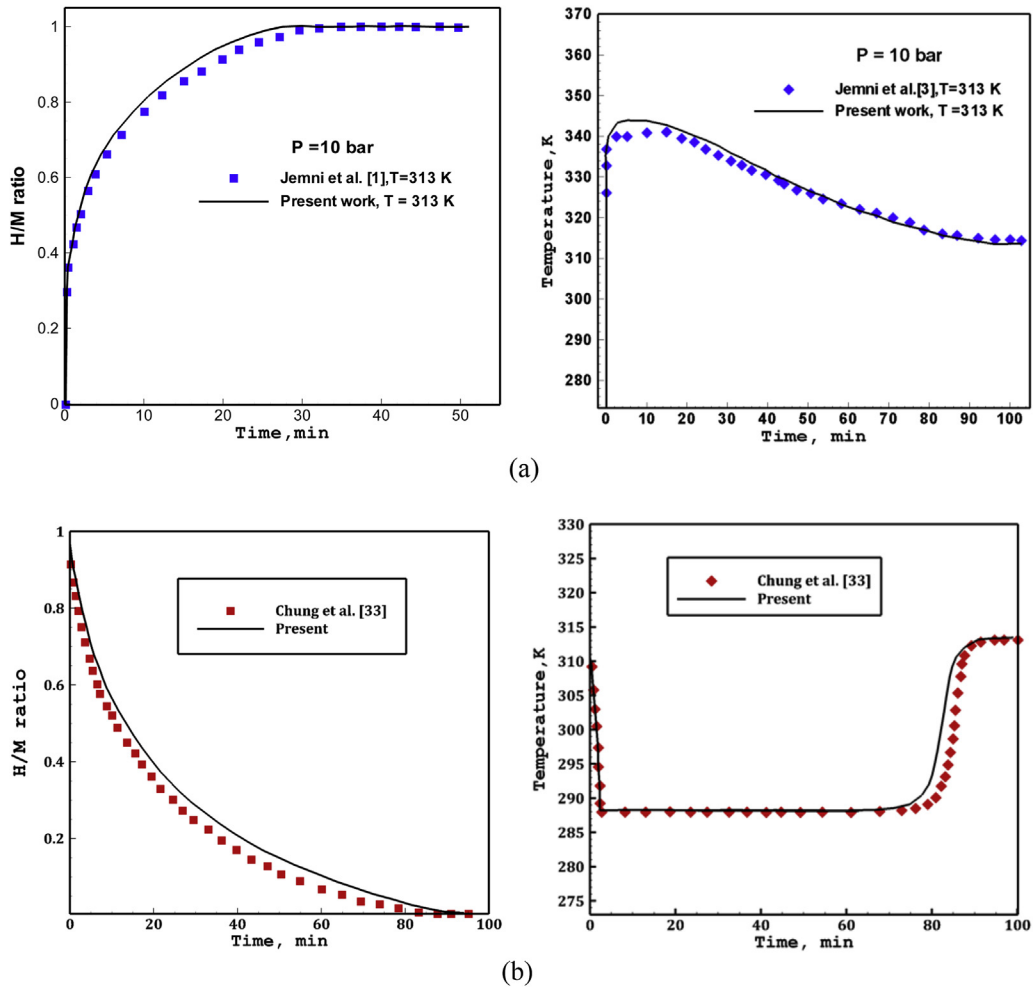

Fig. 2 – Verification of adopted computational model by comparing the H/M ratio and temperature (a) with Jemni et al. work [1] at hydrogen inlet pressure of 10 bar in absorption process (b) with Chung et al. work [33] at discharge pressure of 0.1 MPa and cooling temperature of 313 K in desorption process.

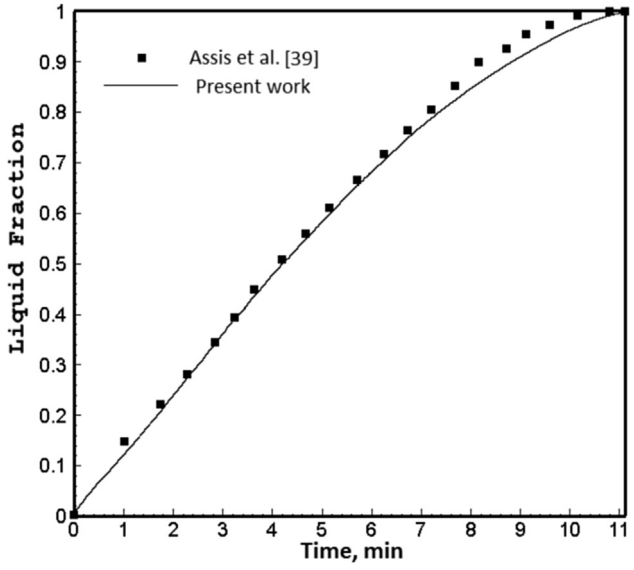

Fig. 3 – Comparison of liquid fraction versus time between present study and Assis et al. [39] work.

absorption, the temperature starts to increase from within a thin layer of PCM near the wall interface while most parts of PCM remain at the initial cool temperature. This is interconnected with the fact that cooling jacket is mostly packed with solid PCM. As time passes, continuing heat transfer from MHT to PCM exceeds the latent heat capacity of phase change material, liquefies it and facilitates the temperature rise in PCM. The heat transfer pattern evolves through time by reducing the high-temperature area in MHT (heat removal) and in turn heating up the PCM in a broader region.

In Fig. 7, the variations of temperature of PCM averaged across both solid and liquid phases are plotted versus time for different supply pressures of hydrogen at $p = 10$, 15 and 20 bar. At initial times ($t < 50$ min) when the reaction rate is considerably high, solid PCM absorbs a large amount of heat from the reacting metal bed and parts of the solid PCM melt. This well describes the abrupt increase in PCM mean temperature regarding the fact that a relatively high temperature area is encompassed only within a limited liquid PCM region (see Fig. 6). As time progresses, the reaction rate in MHT reduces

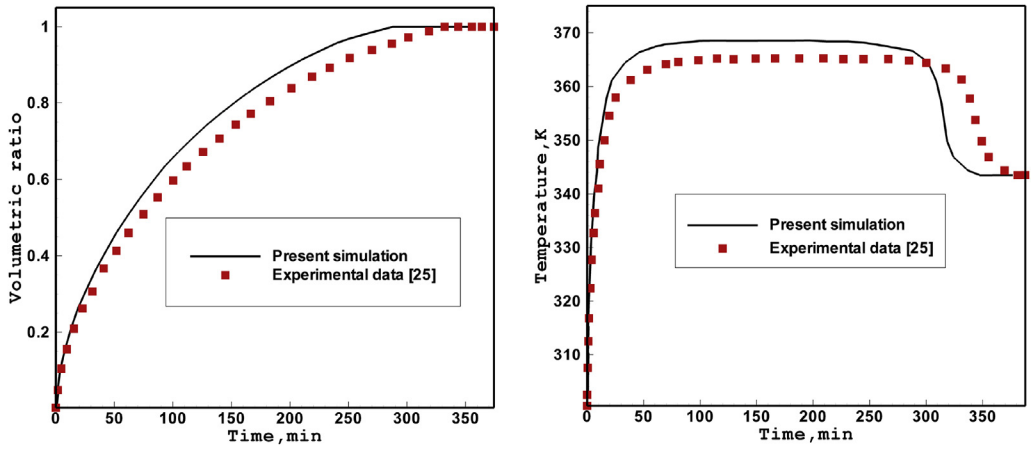

Fig. 4 – Comparison of volume ratio of hydrogen and bed temperature between present simulation and experimental results during charging process at inlet pressure of 1 MPa and initial temperature of 300 K.

and therefore the heat absorbed by the PCM decreases. In this condition, the PCM mean temperature reaches its maximum at $t = 76$, 63 and 54 min respectively for studied pressures of $p = 10$, 15 and 20 bar. Further reduction of reaction rate in MHT and heat absorption by PCM approach their values to zero within the time interval $250 < t < 270$ min. This results in mean temperature reduction to a steady state value at $T = 303.8$ K where solid and liquid PCMs reach thermal equilibrium. During this process, there is still heat transfer from the warm liquid PCM to the cooler solid PCM while their mean temperature remains constant. It is worth noting that faster reaction rate at higher supply pressures accelerates reaching the steady-state thermal equilibrium.

Time-dependent evolution of PCM melt fraction is shown by contours at supply pressure of 10 bar during the time interval $2 \leq t \leq 250$ min in Fig. 8. More solid PCM liquefies through time as larger amount of heat is transferred from reacting MHT to the jacket. It is also obvious from the contours that the interface between solid and liquid phases recedes from the separating wall. This complies with PCM temperature contours (Fig. 6) in which the shrinking region with initial cold temperature exactly matches the area filled by solid PCM.

The time variations of PCM liquid fraction for studied supply pressure range $10 < p < 20$ bar are shown in Fig. 9. Contrary to abrupt rises in PCM temperature plots (Fig. 7), the moderate rate of liquefaction proves its lower response time to the amount of heat absorbed. By increasing the supply pressure of hydrogen, liquid fraction increases due to the higher reaction rate in MHT and temperature in PCM. The liquid fraction approaches to 0.8 for all cases at $t = 250$ min revealing that the amount of initial solid PCM is 20% more than sufficient to absorb the whole generated heat in metal hydride bed with porosity of 0.5.

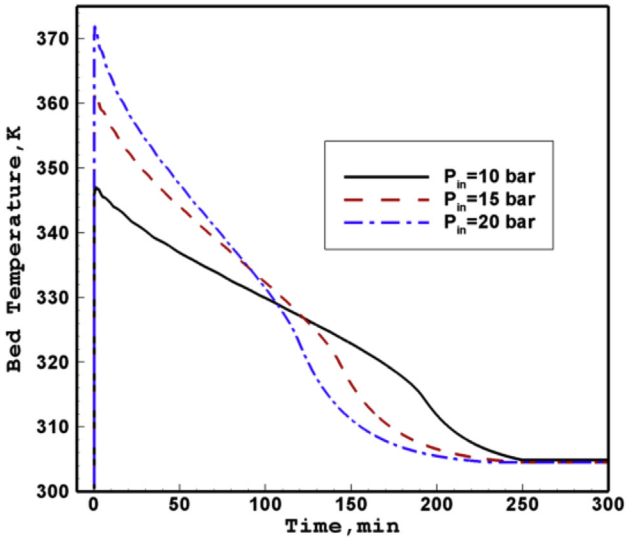

Fig. 5 – Mean temperature variation of metal hydride bed versus time for different supply pressures of $p = 10$, 15 and 20 bar and the bed porosity of $\varepsilon = 0.5$.

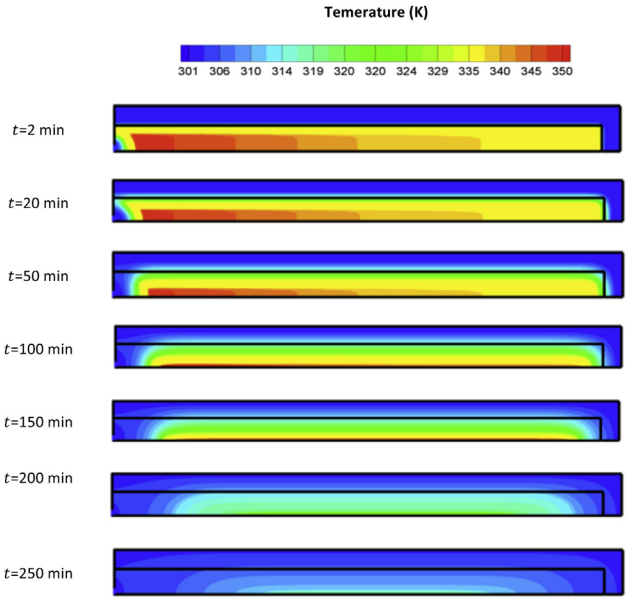

Fig. 6 – Time evolution of system temperature contours at supply pressure of 10 bar during the time interval $2 \leq t \leq 250$ min.

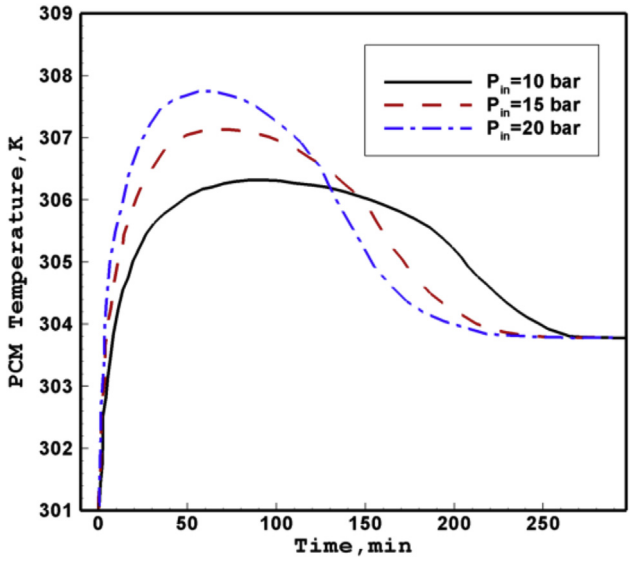

Fig. 7 – Temporal variation of PCM mean temperature (K) at supply pressures of $p = 10$, 15 and 20 bar. The plot covers the heat transfer startup until the steady state is reached.

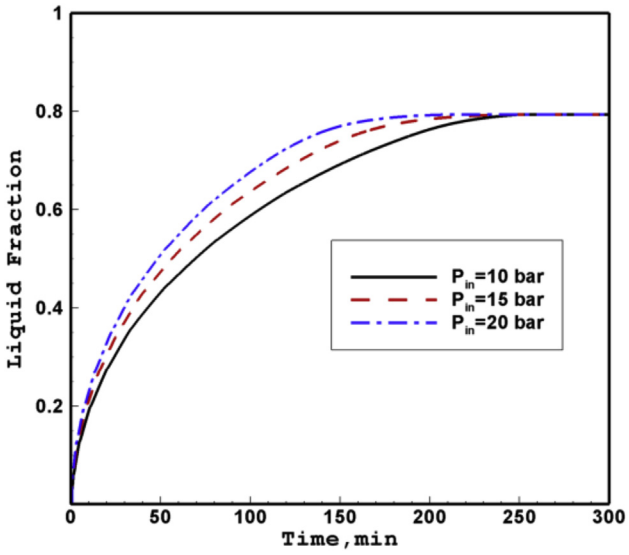

Fig. 9 – Variation of PCM melt fraction versus time at studied supply pressures for hydrogen, $p = 10$, 15 and 20 bar.

The variation of hydrogen to metal (H/M) ratio versus time is plotted in Fig. 10 for the studied range of supply pressures ($10 < p < 20$ bar). Increasing the supply pressure intensifies the mass absorption rate and absorption of hydrogen in the metal bed, and consequently the concentration of H_2 or H/M ratio rises versus pressure. The reaction is driven by the difference between bed pressure (p_g) and equilibrium pressure (p_{eq}), and the difference between saturated density (ρ_{sat}) and density of the empty porous bed (ρ_{emp}). The equilibrium pressure increases by the rise of temperature, according to Van't Hoff equation (Eq. (5)). The density of empty bed approaches quicker to the saturated density for cases with higher reaction rate. This is equivalent to faster approach of H/M ratio to unity where the metal bed is fully saturated. Hence, cases with high supply pressure absorb hydrogen faster than cases with low pressure which is highly important in reducing the absorption time.

The metal bed ($LaNi_5$) undergoes various thermodynamic processes to absorb H_2 and turn into metal hydride ($LaNi_5H_6$) with different characteristics. At early times where hydrogen to metal (H/M) ratio is small, H_2 is absorbed in metal as a heterogeneous solid solution. As H/M ratio increases the stable homogeneous metal hydride nucleates and becomes widespread throughout the bed.

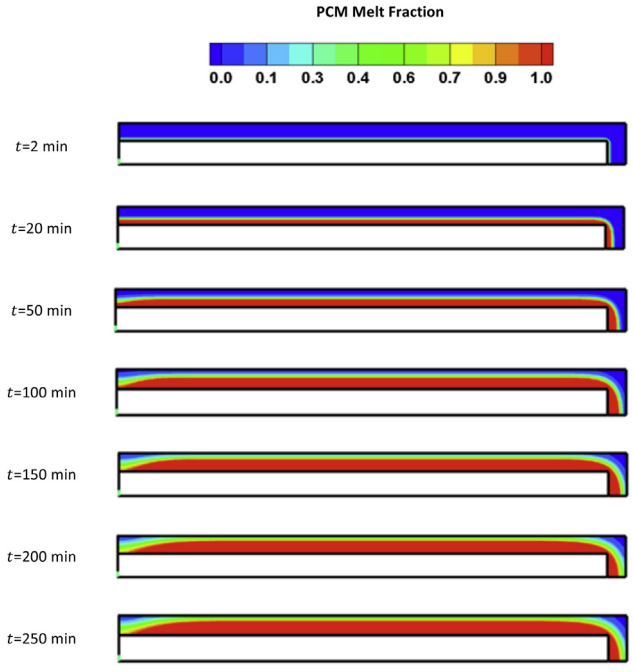

Fig. 8 – Temporal evolution of PCM melt fraction at supply pressure of 15 bar during the time interval $2 \le t \le 250$ min.

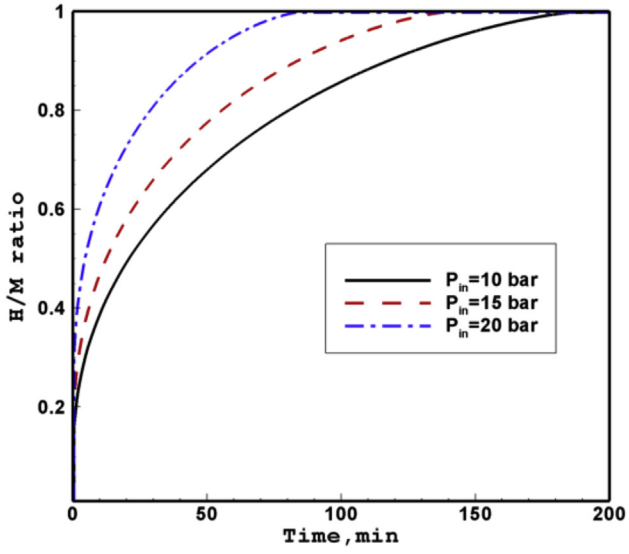

Fig. 10 – Time variation of H/M ratio under the hydrogen supply pressures of 10, 15 and 20 bar.

Structural properties of porous metal hydride greatly affects the H_2 absorption and desorption times, and also the heat transfer through such exothermic and endothermic processes. The packing structure of MHTs (porosity, coordination number, and contact angle) highly influences the effective thermal conductivity of a packed bed [42]. A few researches have addressed the importance of porosity in metal hydride beds. A simulation study performed by Gondor and Lexcellent [43] indicated that for constant values of thermal conductivity, an increase in porosity continuously decreases the MHT charge time. Phate et al. [44] studied the effect of porosity on the absorption time of the metal hydride tank. It was reported that as the porosity increases both the maximum temperature of bed and the time to reach equilibrium are increased. This happens because at low porosities the corresponding thermal conductivity is high, and hence the heat transfer is enhanced more effectively from/to MHT. This effect was shown through H_2 concentration profiles in which longer time for saturation was observed for metal beds with higher porosities.

Fig. 11 studies the effect of bed porosity on H/M ratio, the mean temperature of metal bed, and liquid fraction of PCM at supply pressure of 10 bar. The prominent feature is the faster

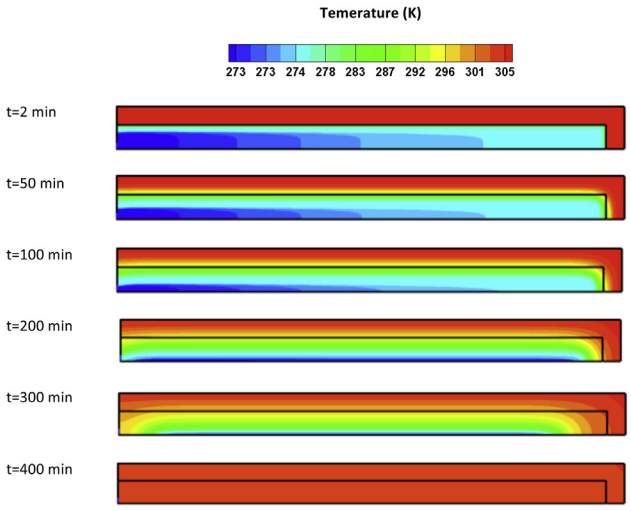

Fig. 12 – Temporal evolution of system temperature contours at discharge pressure of 1.5 bar during the time interval $2 \leq t \leq 400$ min.

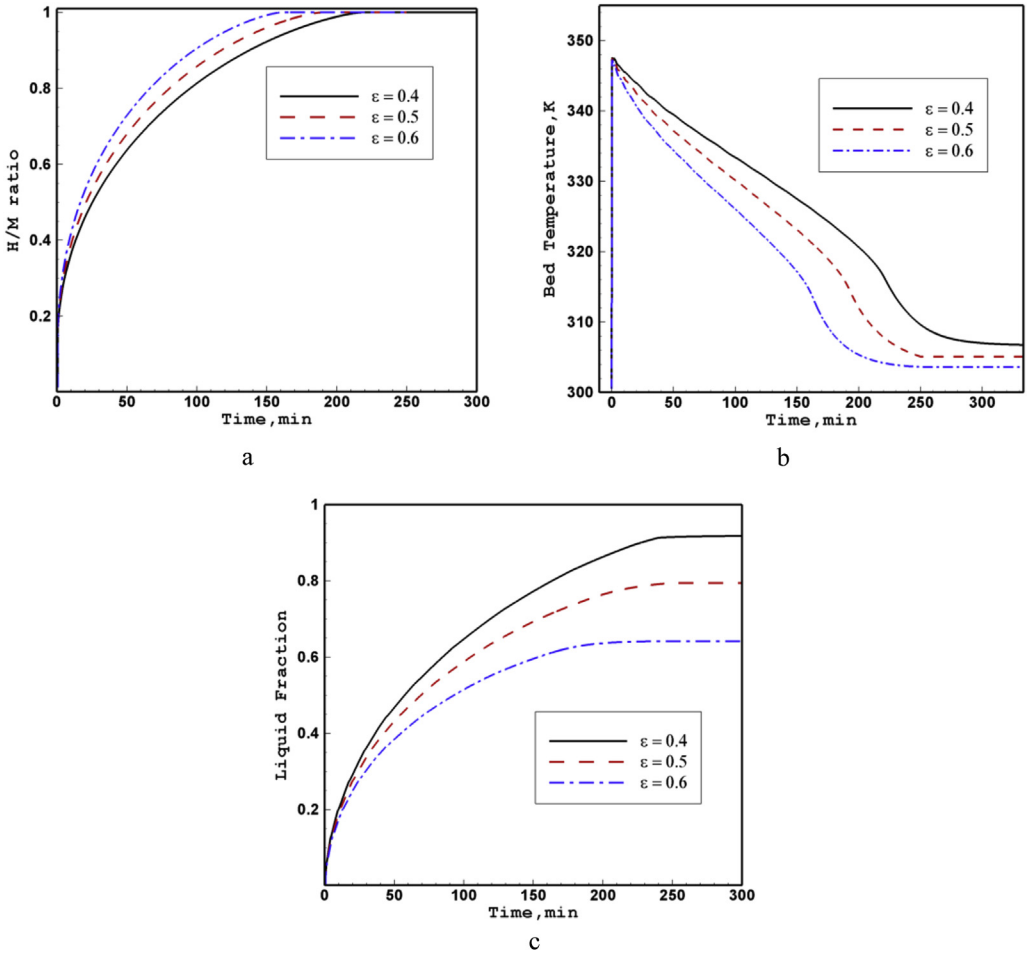

Fig. 11 – Time variations of (a) H/M ratio, (b) metal bed temperature, and (c) PCM liquid fraction for different bed porosities of $\varepsilon = 0.4$, 0.5 and 0.6 at supply pressure of 10 bar. The graphs for each case are continued in time until the steady state is reached.

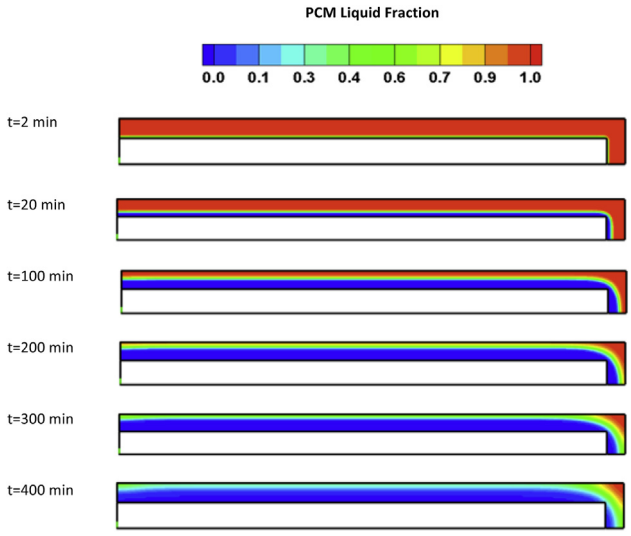

Fig. 13 – Temporal evolution of PCM liquid fraction at discharge pressure of 1.5 bar during the time interval $2 \leq t \leq 400$ min.

hydrogen charge as the MHT porosity increases from $\varepsilon = 0.4$ to 0.6. It should be mentioned that the heat source term in energy equation (Eq. (10)) depends on the porosity and mass absorption rate which itself changes with porosity according to Eq. (2). Hence, the released heat during absorption indirectly correlates with porosity by second order. This explains the MHT temperature decline and faster approach to thermal equilibrium as the bed porosity increases. As the result, PCM melt fraction behaves similarly such that lower porosity leads to higher liquid fraction and slower approach to steady state.

Desorption process

Time-dependent evolution of metal hydride bed and PCM temperature contours is shown at discharge pressure of 1.5 bar and porosity of 0.5 in Fig. 12. The initial temperature of system is set to 305.15 K. A large difference of temperature exists between metal hydride bed and PCM jacket at early time when the reaction rate is high. PCM can release a large amount of heat as latent heat of fusion at the constant temperature. Then the temperature of PCM does not change significantly until whole PCM becomes solid. It can be seen that there is a stratification of temperature along z-axis in

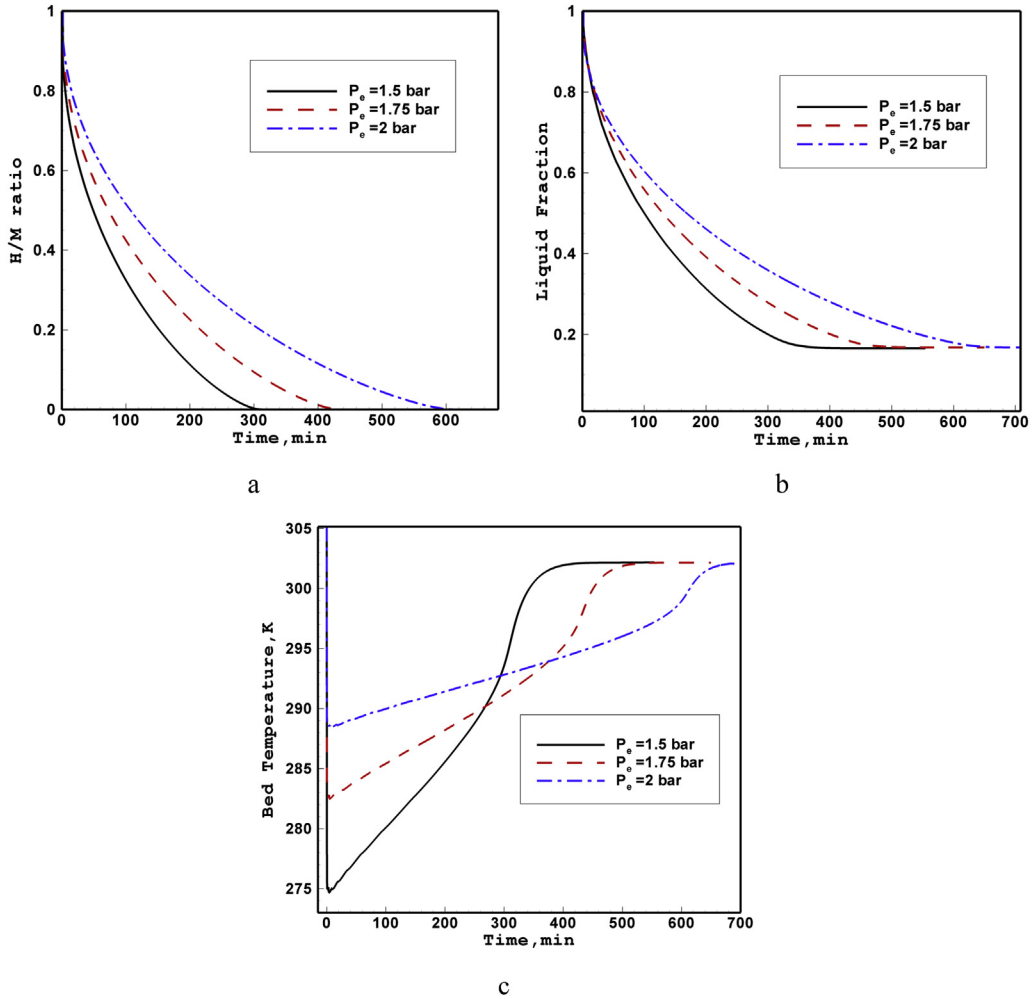

Fig. 14 – Time variations of (a) H/M ratio, (b) metal bed temperature, and (c) PCM liquid fraction for different discharge pressures at bed porosity of 0.5.

addition along r-direction inside metal hydride bed. It reveals that the reaction rate inside long metal hydride bed is higher for region near outlet and it is lower for region far from the outlet. By progressing time, the temperature increases in all over the metal bed due to lowering the reaction rate.

Fig. 13 depicts the melt fraction contour at different time during desorption process with pressure of 1.5 bar. It can be seen that a thin layer of liquid PCM is solidified at early time due to transferring heat from liquid PCM to metal hydride bed. The thickness of solid layer gets thicker by progressing more time. After 300 min, there is not significant change in the thickness of solid layer due to decreasing reaction rate in metal hydride bed. At the end of process (t = 400 min), there is a thin layer of unsolid PCM. It reveals that the amount of PCM is a bit more than it needs for full discharging of metal hydride bed with porosity of 0.5.

The time variation of H/M ratio, liquid fraction and average metal hydride bed temperature for studied discharge pressures are illustrated in Fig. 14. Similar to absorption process, the reaction rate between hydrogen and MHT is high at the beginning of desorption process and then the temperature of metal bed decreases abruptly. The bed temperature reduces more at lower discharging pressure. By decreasing the discharge pressure, the difference between discharge and equilibrium pressures becomes bigger and then the reaction rate gets higher. The full discharge time are occurred at 300, 420 and 600 min for discharge pressures of 1.5, 1.75 and 2 bars, respectively. After these time, the bed temperatures reaches steady state at 302 K. Liquid fraction reaches 0.167 for all studied pressures. It shows that the amount of PCM is more than sufficient to release heat for full desorption of studied metal hydride tank with porosity of 0.5.

Fig. 15 depicts the effect of bed porosity on liquid fraction of PCM, H/M ratio and metal hydride bed temperature at discharge pressure of 1.5 bar. It can be seen that increasing the bed porosity decreases the H/M ratio due to reducing the reaction rate between hydrogen and metal hydride bed according to Eq. (2) and Eq. (10) (as discussed in pervious section). Lower porosity means higher amount of hydride mass that needs higher heat to release. At the end of reaction, the liquid fractions reach 0.33, 0.167 and 0.046 for bed porosities of 0.6, 0.5 and 0.4, respectively. It can be concluded that the initial amount of PCM is sufficient for full discharging of MHT in all studied bed porosities. The minimum temperature of metal hydride bed does not sensitively change by increasing the porosity. However the final temperature of bed at the end of reaction reduces by decreasing the porosity. It is due to lower liquid fraction of PCM at lower bed porosities that

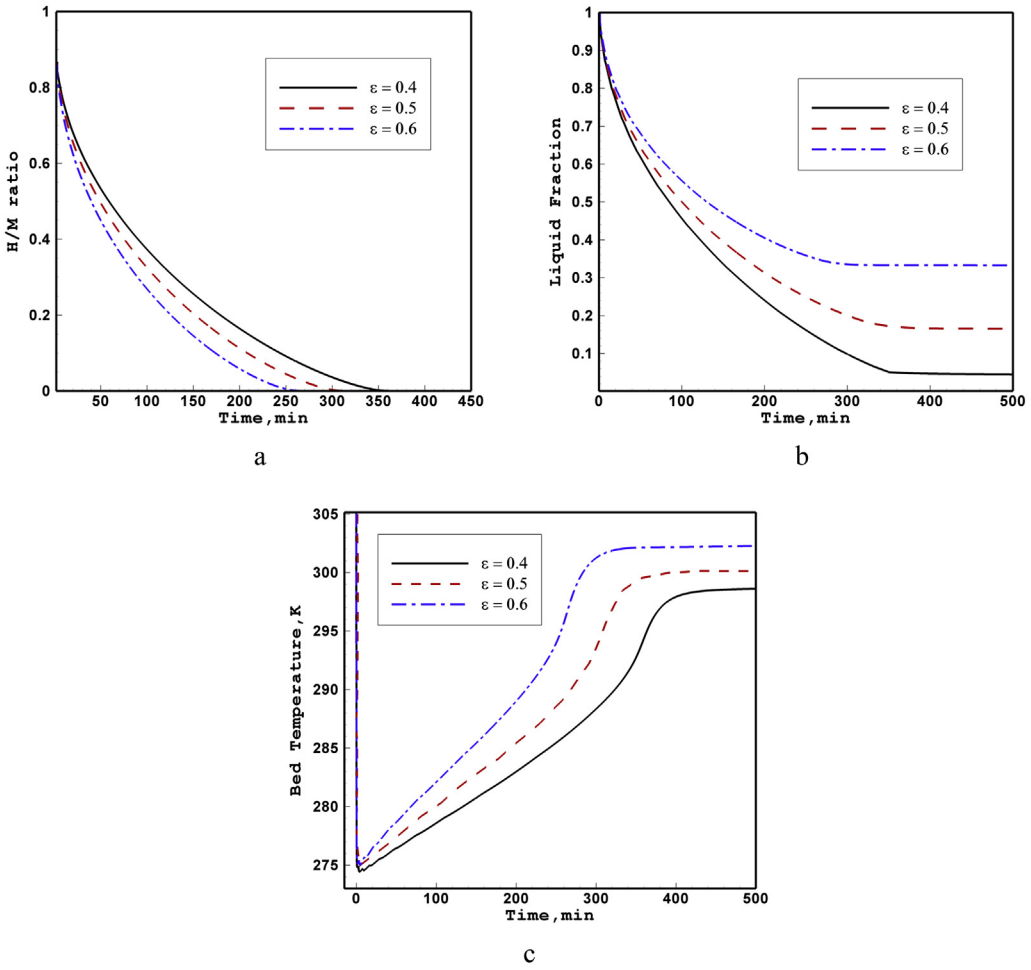

Fig. 15 – Time variations of (a) H/M ratio, (b) PCM liquid fraction, and (c) metal bed temperature for different bed porosities of $\varepsilon = 0.4$, 0.5 and 0.6 at discharge pressure of 1.5 bar.

are thermal equilibrium with metal hydride bed. The temperature of unsolid PCM does not reduces lower than melting temperature. Hence, the final temperature of system decreases by reducing the amount of unsolid PCM.

PCM's thermal conductivity effect

The major undesirable property of PCMs is related to their low thermal conductivities. Although the thermal conductivity of salt-type PCM is more than Paraffin type but it is still low even lower than thermal conductivity of metal hydride tank. Different heat transfer enhancement techniques have been implemented by researchers to overcome this deficiency. Some of most applicable methods are the encapsulation of PCM [45], inserting metal foam [46], adding fins [47,48] and recently, dispersing nanoparticles with high thermal conductivities [49–52]. Adding fins or metal foam augment the effective of thermal conductivity of PCM significantly while they suppress the natural convection by blocking the flow in the PCM with high thermal expansion coefficient or with high volume expansion during phase change. In this way, inserting metal foam is more efficient for using in the salt-type PCM with low thermal expansion and ignorable volume expansion during phase change. Here, it is considered that a metal foam (MF) with porosity of 0.6 inserted in the PCM jacket. The effective thermal conductivity and latent heat of fusion of PCM can be calculated as below:

$$k_{p,eff} = \varepsilon k_p + (1-\varepsilon)k_{mf} \tag{20}$$

$$L_{p,eff} = \varepsilon L_p \tag{21}$$

Fig. 16 provides a comparison of H/M ratio, bed temperature, PCM temperature and liquid fraction between PCM jacket with metal foam and without it during absorption process at supply pressure of 10 bar. It depicts that inserting MF into PCM jacket has significant effect on reducing the charging time. The time of full charging of MHT decrease by 28%. Increasing the thermal conductivity of PCM provides faster heat transfer from MHT. The amount of PCM decrease by inserting metal foam and then as shown in Fig. 16 whole of PCM is melted after 65 min while the reaction is not finished yet. Therefore, the amount of PCM is not enough for absorbing the generated heat from MHT. In this way, the temperature of PCM rise up after melting of whole PCM to absorb remained generated heat in the MHT. The temperature of PCM is reached to about 320 K at the end of process when the steady state is met. Bed temperature drop down faster in comparison with case without metal foam insert. It reaches 320 K at the end of reaction.

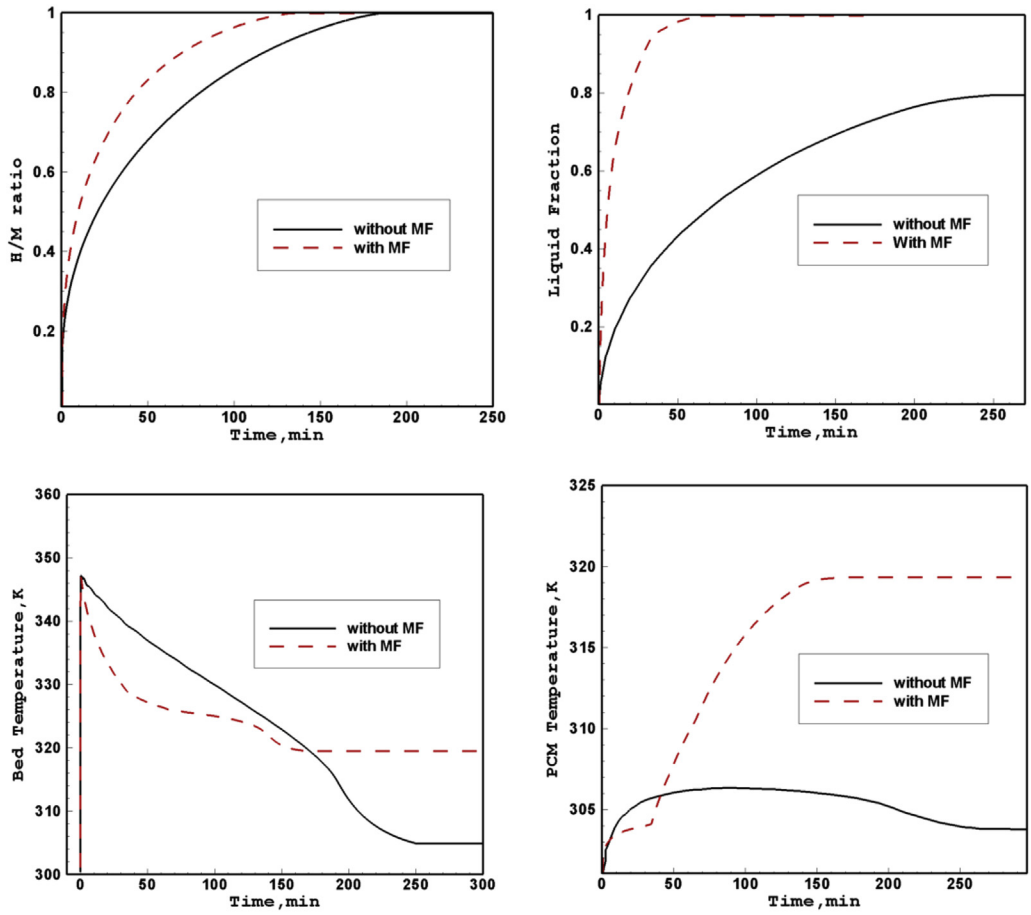

Fig. 16 – The variation of H/M ratio, liquid fraction, bed temperature and PCM temperature versus time during absorption for case with and without metal foam insert in the PCM jacket.

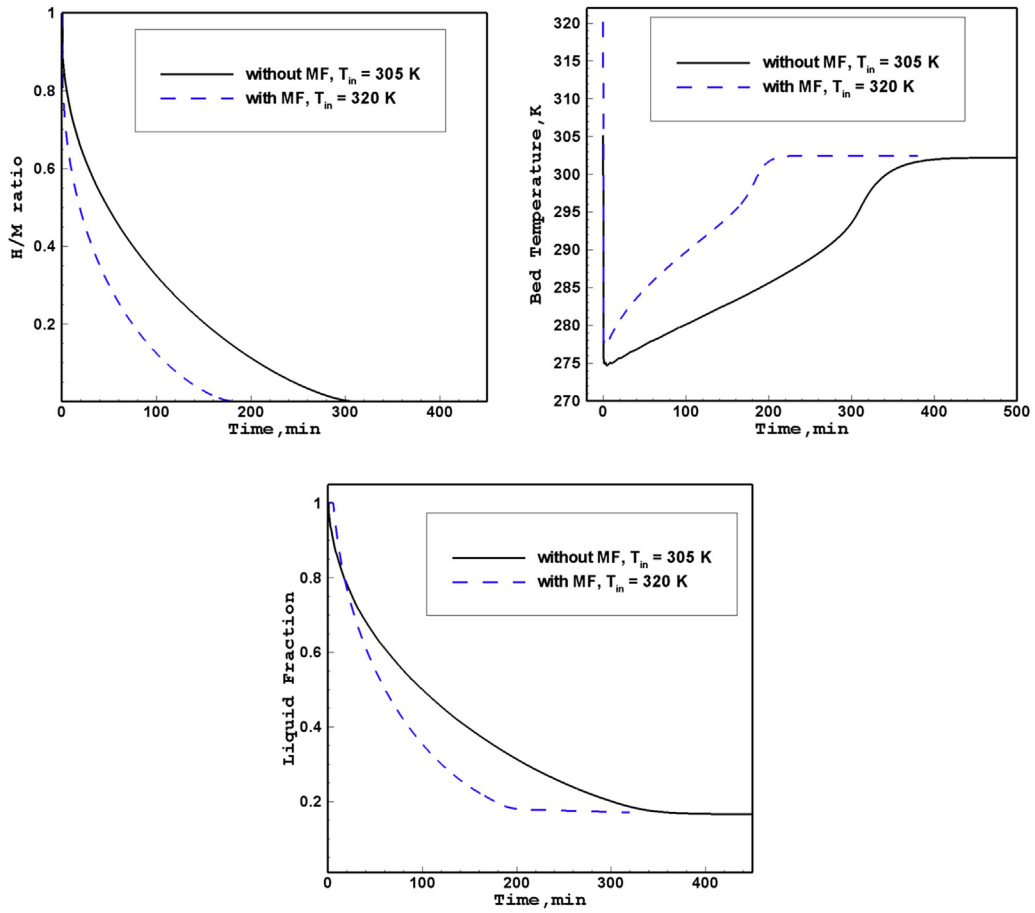

Fig. 17 – The variation of H/M ratio, bed temperature and liquid fraction versus time during desorption for case with and without metal foam insert in the PCM jacket.

The initial temperature of system for desorption process is considered to be 320 K which the system has reached it at the end of absorption process. The variation of H/M ratio, bed temperature and liquid fraction for system with and without metal foam insert is illustrated in Fig. 17. It can be seen that the full desorption time reduces from 300 min to 190 min by inserting metal foam that intensifies the heat transfer rate. The bed temperature drop down less due to the higher initial temperature of system and higher heat transfer rate for case with metal foam. The system reach steady state quicker. The variation of liquid fraction depicts that the amount of unsolid PCM is identical for case with and without metal foam. It is due to sensible energy stored in the PCM at the higher initial temperature.

Conclusion

The charging and discharging processes of hydrogen into/from a tubular $LaNi_5$ metal hydride tank together with the heat transfer to a surrounding annular jacket full of phase change material (PCM) were studied. Elaborate analyses were performed to monitor the time-dependent and local variations of H_2-MHT system temperature, hydrogen to metal (H/M) ratio, and PCM temperature and melt fraction distributions through the PCM jacket versus different H_2 supply/discharge pressures and bed porosities. Important conclusions are drawn as follows

- For absorption process, PCM melt fraction and H/M ratio reach steady state respectively at t = 200, 240 and 258 min for all studied supply pressures (p = 10, 15 and 20 bar). It was noted that systems with higher supply pressure approach steady state faster. Hydrogen reaction rate and consequently the heat absorbed by PCM approach to zero within the time interval 250 < t < 270 min, that all result in steady state, PCM mean temperature of T = 303.8 K. The H/M ratio approaches unity (equivalent to full saturation) quicker at high supply pressures. This can be interpreted as shorter charging time for hydrogen. As the porosity of metal hydride bed rises from ε = 0.4 to 0.6, the H/M ratio or H_2 concentration increases leading to faster absorption times. MHT temperature drops faster at high porosities and reaches the equilibrium quicker. Higher bed porosity leads to lower PCM melt fraction but faster equilibrium.
- For desorption process, the full discharge time are occurred at 300, 420 and 600 min for discharge pressures of 1.5, 1.75 and 2 bars, respectively. System with lower discharge

pressure approaches to steady state faster. Increasing the bed porosities decreases the H/M ratio leading to higher discharging time. Similar to absorption process, MHT temperature reaches the equilibrium quicker at higher bed porosities. Also, the liquid fraction of PCM reduces by decreasing the bed porosities.

- By inserting the metal foam in the PCM jacket, the melting and solidification rate enhances and it cause to reducing the charging and discharging time desirably.

REFERENCES

[1] Jemni A, Nasrallah SB. Study of two-dimensional heat and mass transfer during absorption in a metal-hydrogen reactor. Int J Hydrogen Energy 1995;20:43–52.
[2] Nasrallah SB, Jemni A. Heat and mass transfer models in metal-hydrogen reactor. Int J Hydrogen Energy 1997;22:67–76.
[3] Jemni A, Nasrallah SB, Lamloumi J. Experimental and theoretical study of a metal–hydrogen reactor. Int J Hydrogen Energy 1999;24:631–44.
[4] Muthukumar P, Madhavakrishna U, Dewan A. Parametric studies on a metal hydride based hydrogen storage device. Int J Hydrogen Energy 2007;32:4988–97.
[5] Muthukumar P, Ramana SV. Study of heat and mass transfer in $MmNi_{4.6}Al_{0.4}$ during desorption of hydrogen. Int J Hydrogen Energy 2010;35:10811–8.
[6] Mellouli S, Askri F, Dhaou H, Jemni A, Nasrallah SB. A novel design of a heat exchanger for a metal-hydrogen reactor. Int J Hydrogen Energy 2007;32:3501–7.
[7] Dhaou H, Souahlia A, Mellouli S, Askri F, Jemni A, Nasrallah SB. Experimental study of a metal hydride vessel based on a finned spiral heat exchanger. Int J Hydrogen Energy 2010;35:1674–80.
[8] Muthukumar P, Singhal A, Bansal G. Thermal modeling and performance analysis of industrial-scale metal hydride based hydrogen storage container. Int J Hydrogen Energy 2012;37:14351–64.
[9] Askri F, Salah MB, Jemni A, Nasrallah SB. Optimization of hydrogen storage in metal-hydride tanks. Int J Hydrogen Energy 2009;34:897–905.
[10] MacDonald BD, Rowe AM. Experimental and numerical analysis of dynamic metal hydride hydrogen storage systems. J Power Sources 2007;174:282–93.
[11] Freni A, Cipiti F, Cacciola G. Finite element-based simulation of a metal hydride-based hydrogen storage tank. Int J Hydrogen Energy 2009;34:8574–82.
[12] Chung C, Yang S-W, Yang C-Y, Hsu C-W, Chiu P-Y. Experimental study on the hydrogen charge and discharge rates of metal hydride tanks using heat pipes to enhance heat transfer. Appl Energy 2013;103:581–7.
[13] Kong X, Lu S, Li Y, Huang J, Liu S. Numerical study on the thermal performance of building wall and roof incorporating phase change material panel for passive cooling application. Energy Build 2014;81:404–15.
[14] Persson J, Westermark M. Phase change material cool storage for a Swedish passive house. Energy Build 2012;54:490–5.
[15] Tan F, Fok S. Cooling of helmet with phase change material. Appl Therm Eng 2006;26:2067–72.
[16] Shalaby S, Bek M, El-Sebaii A. Solar dryers with PCM as energy storage medium: a review. Renew Sustain Energy Rev 2014;33:110–6.
[17] Alshaer W, Nada S, Rady M, Del Barrio EP, Sommier A. Thermal management of electronic devices using carbon foam and PCM/nano-composite. Int J Therm Sci 2015;89:79–86.
[18] Weng Y-C, Cho H-P, Chang C-C, Chen S-L. Heat pipe with PCM for electronic cooling. Appl Energy 2011;88:1825–33.
[19] Soares N, Costa J, Gaspar A, Santos P. Review of passive PCM latent heat thermal energy storage systems towards buildings' energy efficiency. Energy Build 2013;59:82–103.
[20] Darzi AR, Moosania S, Tan F, Farhadi M. Numerical investigation of free-cooling system using plate type PCM storage. Int Commun Heat Mass Transf 2013;48:155–63.
[21] Hosseinizadeh S, Darzi AR, Tan F, Khodadadi J. Unconstrained melting inside a sphere. Int J Therm Sci 2013;63:55–64.
[22] Tay N, Bruno F, Belusko M. Experimental investigation of dynamic melting in a tube-in-tank PCM system. Appl Energy 2013;104:137–48.
[23] Mahmoud S, Tang A, Toh C, Raya A-D, Soo SL. Experimental investigation of inserts configurations and PCM type on the thermal performance of PCM based heat sinks. Appl Energy 2013;112:1349–56.
[24] Kozak Y, Abramzon B, Ziskind G. Experimental and numerical investigation of a hybrid PCM–air heat sink. Appl Therm Eng 2013;59:142–52.
[25] Garrier S, Delhomme B, De Rango P, Marty P, Fruchart D, Miraglia S. A new MgH_2 tank concept using a phase-change material to store the heat of reaction. Int J Hydrogen Energy 2013;38:9766–71.
[26] Mellouli S, Khedher NB, Askri F, Jemni A, Nasrallah SB. Numerical analysis of metal hydride tank with phase change material. Appl Therm Eng 2015;90:674–82.
[27] Mâad HB, Askri F, Nasrallah SB. Heat and mass transfer in a metal hydrogen reactor equipped with a phase-change heat-exchanger. Int J Therm Sci 2016;99:271–8.
[28] Mâad HB, Miled A, Askri F, Nasrallah SB. Numerical simulation of absorption-desorption cyclic processes for metal-hydrogen reactor with heat recovery using phase-change material. Appl Therm Eng 2016;96:267–76.
[29] Kim J-K, Park I-S, Kim KJ, Gawlik K. A hydrogen-compression system using porous metal hydride pellets of LaNi5-xAlx. Int J hydrogen energy 2008;33:870–7.
[30] Klein H-P, Groll M. Development of a two-stage metal hydride system as topping cycle in cascading sorption systems for cold generation. Appl Therm Eng 2002;22:631–9.
[31] Fedorov E, Shanin Y, Izhvanov L. Simulation of hydride heat pump operation. Int J Hydrogen Energy 1999;24:1027–32.
[32] Willers E, Wanner M, Groll M. A multi-hydride thermal wave device for simultaneous heating and cooling. J Alloys Compd 1999;293:915–8.
[33] Chung C, Ho C-J. Thermal–fluid behavior of the hydriding and dehydriding processes in a metal hydride hydrogen storage canister. Int J Hydrogen Energy 2009;34:4351–64.
[34] Sandrock G, Thomas G. The IEA/DOE/SNL on-line hydride databases. Appl Phys A 2001;72:153–5.
[35] Patankar S. Numerical heat transfer and fluid flow. CRC Press; 1980.
[36] Voller VR, Prakash C. A fixed grid numerical modelling methodology for convection-diffusion mushy region phase-change problems. Int J Heat Mass Transf 1987;30:1709–19.
[37] Versteeg HK, Malalasekera W. An introduction to computational fluid dynamics: the finite volume method: Pearson education. 2007.
[38] Voller V, Brent A, Reid K. Computational modelling framework for analysis of metallurgical solidification processes and phenomena. The Institute of Metals; 1988. p. 378–80.
[39] Assis E, Katsman L, Ziskind G, Letan R. Numerical and experimental study of melting in a spherical shell. Int J Heat Mass Transf 2007;50:1790–804.

[40] Jiao K, Li X, Yin Y, Zhou Y, Yu S, Du Q. Effects of various operating conditions on the hydrogen absorption processes in a metal hydride tank. Appl Energy 2012;94:257–69.
[41] Nam J, Ko J, Ju H. Three-dimensional modeling and simulation of hydrogen absorption in metal hydride hydrogen storage vessels. Appl Energy 2012;89:164–75.
[42] Matsushita M, Monde M, Mitsutake Y. Experimental formula for estimating porosity in a metal hydride packed bed. Int J Hydrogen Energy 2013;38:7056–64.
[43] Gondor G, Lexcellent C. Analysis of hydrogen storage in metal hydride tanks introducing an induced phase transformation. Int J Hydrogen Energy 2009;34:5716–25.
[44] Phate AK, Maiya MP, Murthy SS. Simulation of transient heat and mass transfer during hydrogen sorption in cylindrical metal hydride beds. Int J Hydrogen Energy 2007;32:1969–81.
[45] Kousksou T, Bruel P. Encapsulated phase change material under cyclic pulsed heat load. Int J Refrig 2010;33:1648–56.
[46] Zhang P, Meng Z, Zhu H, Wang Y, Peng S. Experimental and numerical study of heat transfer characteristics of a paraffin/metal foam composite PCM. Energy Procedia 2015;75:3091–7.
[47] Mat S, Al-Abidi AA, Sopian K, Sulaiman MY, Mohammad AT. Enhance heat transfer for PCM melting in triplex tube with internal–external fins. Energy Convers Manag 2013;74:223–36.
[48] Li Z, Wu Z-G. Analysis of HTFs, PCMs and fins effects on the thermal performance of shell–tube thermal energy storage units. Sol Energy 2015;122:382–95.
[49] Alshaer W, Nada S, Rady M, Le Bot C, Del Barrio EP. Numerical investigations of using carbon foam/PCM/Nano carbon tubes composites in thermal management of electronic equipment. Energy Convers Manag 2015;89:873–84.
[50] Hosseinizadeh S, Darzi AR, Tan F. Numerical investigations of unconstrained melting of nano-enhanced phase change material (NEPCM) inside a spherical container. Int J Therm Sci 2012;51:77–83.
[51] Jourabian M, Farhadi M, Darzi AAR. Outward melting of ice enhanced by Cu nanoparticles inside cylindrical horizontal annulus: Lattice Boltzmann approach. Appl Math Model 2013;37:8813–25.
[52] Ali Rabienataj Darzi A, Farhadi M, Jourabian M, Vazifeshenas Y. Natural convection melting of NEPCM in a cavity with an obstacle using lattice Boltzmann method. Int J Numer Methods Heat Fluid Flow 2013;24:221–36.
[53] Fluent, Inc.. Fluent 6.0.12 User's guide. Fluent, Inc.. Lebanon, NH 03766, USA: Centerra Resource Park, 10 Cavendish Court; 2001.